Effect of fluoride on the thickness, surface roughness and corrosion resistance of titanium anodic oxide films formed in a phosphate buffer solution at different applied potentials

Efeito do flúor na espessura, rugosidade da superfície e resistência à corrosão de filmes de óxido anódico de titânio formados em uma solução tampão fosfato m diferentes potenciais aplicados

Efecto del fluoruro sobre el espesor, la rugosidad de la superficie y la resistencia a la corrosión de las películas de óxido anódico de titanio formadas en una solución tampón de fosfato a diferentes potenciales aplicados

Gláucia Domingues

ORCID: https://orcid.org/0000-0003-3189-4249

Centro Federal de Educação Tecnológica Celso Suckow da Fonseca, Brazil

E-mail: glaucia.domingues@cefet-rj.br

Michele de Almeida Oliveira

ORCID: https://orcid.org/0000-0002-5162-0299

Universidade Federal Fluminense, Brazil

E-mail: oliveiraalmeidamichele@gmail.com

Nayne Barros Gonzaga Ferreira

ORCID: https://orcid.org/0000-0002-9787-645X

Universidade Federal Fluminense, Brazil

E-mail: naynegonzaga@id.uff.br

Bhetina Cunha Gomes

ORCID: https://orcid.org/0000-0003-1603-7193

Universidade Federal Fluminense, Brazil

E-mail: bhetinagomes@id.uff.br

Elivelton Alves Ferreira

ORCID: https://orcid.org/0000-0001-6991-6558

Universidade Federal Fluminense, Brazil

E-mail: eliveltonalves@id.uff.br

Ladário da Silva

ORCID: https://orcid.org/0000-0003-1643-7840

Universidade Federal Fluminense, Brazil

E-mail: ladariosilva@id.uff.br

Abstract

The anodizing process and anions type present in the electrolyte during anodic oxidation are important parameters to improve oxide biocompatibility. From these parameters, it is possible to control the thickness and surface roughness of the oxide film. This control is of major importance, once blood clots can be avoided when the oxide film on the metal substrate has a small surface roughness (Ra ≤ 50 nm). In this paper, the thickness, surface roughness, and corrosion resistance of the anodized titanium film were studied in a phosphate buffer solution containing fluoride anions (0.6 w.t % NaF), at 20 V, 40 V, 60 V, and 80 V, using atomic force microscopy (AFM), spectroscopic ellipsometry (SE), and electrochemical impedance spectroscopy (EIS) techniques. It was observed that thickness and roughness tend to increase as the applied potential rises. For oxides grown in the solution without NaF, the growth rate is roughly 1.3 ± 0.2 nm/V. Surface roughness generally presents the same behaviour. Moreover, EIS and SE thickness measurements agree at 20 V and 60 V but disagree at 80 V. This may be associated with a possible dielectric breakdown at 80 V. The oxide film formed at 60 V showed the best corrosion resistance in relation to the other studied potentials. Globular structures were also observed using AFM on surfaces at 40 V, 60 V, and 80 V, which suggests oxide film nucleation. Oxide films formed in solution with NaF presented lower thickness, excellent corrosion resistance, and low surface roughness (Ra ≤ 50 nm).

Keywords: Titanium oxide; Fluoride; Thickness; Surface roughness; Corrosion resistance.

Resumo

O processo de anodização e o tipo de ânions presentes no eletrólito durante a oxidação anódica são parâmetros importantes para melhorar a biocompatibilidade do óxido. A partir desses parâmetros, é possível controlar a espessura e a rugosidade superficial do filme de óxido. Esse controle é muito importante, visto que a formação de coágulos sanguíneos pode ser evitada quando o filme de óxido no substrato metálico apresenta pequena rugosidade superficial (Ra ≤ 50 nm). Neste trabalho, a espessura, rugosidade superficial e resistência à corrosão do filme de titânio anodizado foram estudados em solução tampão de fosfato contendo ânions fluoreto (0,6% em peso de NaF), a 20 V, 40 V, 60 V e 80 V, usando técnicas

de microscopia de força atômica (AFM), elipsometria espectroscópica (ES) e espectroscopia de impedância eletroquímica (EIE). Observou-se que a espessura e a rugosidade tendem a aumentar com o aumento do potencial aplicado. Para óxidos crescidos na solução sem NaF, a taxa de crescimento é de aproximadamente 1,3 ± 0,2 nm/V. A rugosidade superficial geralmente apresenta o mesmo comportamento. Além disso, as medidas de espessura de EIE e ES concordaram em 20 V e 60 V, mas discordaram em 80 V. Isso pode estar associado a uma possível quebra dielétrica em 80 V. O filme de óxido formado em 60 V apresentou a melhor resistência à corrosão em relação aos outros potenciais estudados. Estruturas globulares foram observadas usando AFM em superfícies a 40 V, 60 V e 80 V, o que sugere nucleação de filme de óxido. Filmes de óxido formados em solução com NaF apresentaram menor espessura, excelente resistência à corrosão e baixa rugosidade superficial (Ra ≤ 50 nm).

Palavras-chave: Óxido de titânio; Fluoreto; Espessura; Rugosidade superficial; Resistência à corrosão.

Resumen

El proceso de anodización y el tipo de aniones presentes en el electrolito durante la oxidación anódica son parámetros importantes para mejorar la biocompatibilidad del óxido. A partir de estos parámetros, es posible controlar el espesor y la rugosidad de la superficie de la película de óxido. Este control es muí importante, una vez que se pueden evitar los coágulos de sangre cuando la película de óxido sobre el sustrato metálico tiene una pequeña rugosidad superficial (Ra ≤ 50 nm). En este artículo, se estudiaron el grosor, la rugosidad de la superficie y la resistencia a la corrosión de la película de titanio anodizado en una solución tampón de fosfato que contiene aniones fluoruro (0,6% en peso de NaF), a 20 V, 40 V, 60 V y 80 V, utilizando microscopía de fuerza atómica (AFM), técnicas de elipsometría espectroscópica (ES) y espectroscopía de impedancia electroquímica (EIE). Se observó que el espesor y la rugosidad tienden a aumentar a medida que aumenta el potencial aplicado. Para los óxidos que crecen en la solución sin NaF, la tasa de crecimiento es de aproximadamente 1,3 ± 0,2 nm/V. La rugosidad superficial presenta generalmente el mismo comportamiento. Además, las mediciones de espesores EIE y ES coinciden a 20 V y 60 V pero discrepan a 80 V. Esto puede estar asociado con una posible ruptura dieléctrica a 80 V. La película de óxido formada a 60 V mostró la mejor resistencia a la corrosión en relación con la otra potenciales estudiados. Se observaron estructuras globulares usando AFM en superficies a 40 V, 60 V y 80 V, lo que sugiere la nucleación de la película de óxido. Las películas de óxido formadas en

solución con NaF presentaron menor espesor, excelente resistencia a la corrosión y baja rugosidad superficial (Ra ≤ 50 nm).

Palabras clave: Óxido de titanio; Fluoruro; Grosor; Rugosidad de la superficie; Resistencia a la corrosión.

1. Introduction

Titanium and its alloys usually are biocompatible (Aladjem, 1973). Properties such as biocompatibility and corrosion resistance are due to the spontaneous formation of a chemically stable oxide on its surface (Aladjem, 1973). This naturally grown film is mainly amorphous and very thin, presenting a thickness generally in the scale of nanometers (Mazzarolo et al., 2012). According to Vera et al. (2017), they also present a high density of defects in native oxide film, which can decrease their corrosion resistance, depending on the conditions and environment. These defects can be reduced by oxide film thickening using oxidation techniques such as anodization (Simka et al., 2011; Diamanti & Pedeferri, 2007; Liao et al., 2017).

Titanium anodic films are obtained generally using either phosphoric or sulfuric acid electrolytes, and alkali solutions (Karambakhsh et al., 2011; Saldanha et al., 2020; Huang & Liu,2013; Marino et al., 2004). Characterization of the oxides films that are grown a in phosphate buffer solution of pH equal 6.5 needs to be studied more deeply (Marino et al., 2004). The dependence between anodizing technique, surface treatment condition, and anions present into electrolyte during anodic oxidation is the subject of many studies in this area (Xing et al., 2013; Ohtsu et al., 2014). However, some anions present in corrosive environments at different pH values can change the passive film stability condition of the called valve metals like titanium (Robin & Meirelis, 2007). Kong (2008) studied the effect of fluoride contained in 1.0 mol L^{-1} perchloric acid solution on the stability of the anodic oxide films obtained by anodization, and observed that above a critical concentration value of fluoride equal to 0.001 mol L^{-1}, a passive breakdown could occur. Beyond that, it is known that fluoride anions may lead to the breakdown of passive film formed on the surface of titanium in some aqueous solutions mainly at lower pH values (Wang et al., 2016; Fukushima et al., 2018; Fovet et al., 2001). Tsuchiya et al. (2006) showed that lower pH values on fluoride media promote competition between the growth and dissolution of the oxide film, allowing nanotube shaped oxides to be formed. Zhai et al. (2019) argue that titanium and its alloys present good mechanical properties as well as good biocompatibility, but they have no

antbacterial activity, what may hinder its use. They consider using fluoride anions ($^-$F) on anodization so that the grown film may acquire antibacterial activity. Another important factor is the coating roughness. The promotion of blood clots, which can lead to thrombosis, can be avoided when the biocompatible metal has a low surface roughness (coating roughness) (Ra ≤ 50 nm) (Vera et al., 2017).

The color is attributed to the interference of light, thence, the observed color is the visual representation of the thickness of the transparent oxide film that caused it. The colors are generated by the interference of multiple beams of light in the transparent anodic oxide films on metals (Pedeferri, 2015).

To access thickness, surface roughness, and corrosion resistance, a few techniques were used. Ellipsometry (Fujiwara, 2007) is a non-destructive technique that allows us to sense the optical properties of thin films, which ultimately allow us to determine their thickness. This technique can access the refractive index (n), the extinction coefficient (k), and the film thickness. Ellipsometry also relies on the analysis of the change of the polarization state of incident light upon interaction and reflection on the sample surface. Ellipsometric parameters tan(Ψ) and cos(Δ) capture information of the ratios of the polarized reflected and incident electric field components, and phase changes upon reflection, respectively (Fujiwara, 2007). These parameters were measured and used with an optical model of the material built using a proprietary software (Csermely et al., 2012) to generate the simulated (modeled) ellipsometric parameters. So, it is possible to compare the measured parameters with the simulated ones. The closer the measured and the simulated are, the better. This technique has been used in studies about optical parameters, oxide layer thickness related to electrochemical behaviour of titanium and its alloys, mainly in acidic or alkaline environments (Mardare & Hones, 1999; Blackwood et al., 1989). Atomic force microscopy (AFM) is a well-known and widely used technique to investigate the roughness and surface topography of the samples (Saldanha et al., 2020; Huang & Liu, 2013; Zhai et al., 2019).

Electrochemical impedance spectroscopy (EIS), a technique used to study the metal/oxide film/electrochemical solution system (Simka et al., 2011; Diamanti & Pedeferri, 2007; Saldanha et al., 2020), was employed to evaluate the corrosion resistance and to estimate the thickness of titanium anodized oxide film. Once fluoride incorporation during anodization procedure and the coating roughness can influence the biocompatibility of oxide film on titanium, this work focuses on evaluating the surface roughness, oxide thickness, and corrosion resistance of titanium oxides film obtained at different potentials applied in a phosphate buffer solution, without NaF and with 0.6 w. t % NaF.

2. Materials and Methods

In order to classify the methodology (Pereira et al., 2018) of this research, we can argue that this research is an experimental one, with mainly quantitative approach based on previous both theoretical and experimental researches, published in the literature, and largely cited in this article.

2.1 Surface samples preparation and anodization procedure

2.1.1 Titanium samples

A grade II titanium plaque (Tibrasil Titânio®) was cut into eight samples of dimensions 8 mm x 8 mm x 4 mm using a 10 % oil solution coolant and a thermal pencil for working temperature from 73 °C to 93 °C. The surfaces samples were mechanically grinded with silicon carbide abrasive papers, starting from 80 mesh to 1200 mesh, changing grinding direction as abrasive papers are changed, and carefully avoiding heating, so that temperature did not reach 100 °C. After grinding, the samples were mechanically polished until mirror-like finish was reached, using diamond paste of particle size 3.0 µm and 1.0 µm and proper polishing cloths. Subsequently, samples were cleaned with distilled water and isopropyl alcohol, and afterward, dried in forced air at room temperature.

2.1.2 Anodization Procedure

Titanium samples were anodized in a phosphate buffer solution with pH equal to 6.5 ± 0.2, composed of 0.67 mol.L^{-1} sodium phosphate (Na$_2$HPO$_4$) and of 0.67 mol.L^{-1} potassium phosphate (KH$_2$PO$_4$) to which 1.0 w.t % NaCl of 99.99% purity was added. The used ultra-purified water came from a Milli-Q® device. Four samples were anodized in this solution, and another four were anodized in the same solution with the addition of 0.6 w.t % NaF. In both solutions, a Pt electrode was used as the counter-electrode. The phosphate buffer solution was used to ensure that the electrolyte pH did not change during anodization procedure, and phosphate solution is one of the known buffer mechanisms present in saliva. Moreover, it is known that incorporation of phosphate inside oxide films titanium leads to enhancement of their osteointegration (Simka et al., 2011). Besides that, in this pH value, the titanium oxide film is at passivation conditions according to the Pourbaix diagram (Robin &

Meirelis, 2007). Fluoride and phosphate were used to incorporate those ions into oxide films during growth at high potentials (Saldanha et al., 2020). The titanium anodization procedure was carried out using Instrutherm® DC electrical power supply, model FA-3003, to apply 20 V, 40 V, 60 V and 80 V for 30 s in all potentials. After the anodization, the samples were also rinsed with ultra-pure water and isopropyl alcohol. Table 1 presents the anodizing voltages and the samples names designation.

Table 1. Designation of titanium samples according to the applied voltages for 30 seconds and presence of fluoride anions.

Applied voltage (V)	Phosphate buffer solution without NaF	Phosphate buffer solution 0.6 w.t % NaF
20	A20	A20 F
40	A40	A40 F
60	A60	A60 F
80	A80	A80 F

Source: Authors (2020).

Table 1 specifies the samples and solutions used. The capital F in the sample's name showed in the rightmost column refers to films grown in a phosphate buffer solution containing 0.6 w.t % NaF.

2.2 Spectroscopic ellipsometry

The GES5-E Semilab® ellipsometer controlled by SOPRA® R&D software was used to study the titanium oxide obtained by anodizing procedures. The measurements were made using an incidence angle of 75º in the wavelength range between 250 and 1000 nm. Light source is a non-polarized Xenon lamp with a rotating polarizer, and microspots (collimating lens). Modelling was accomplished using the proprietary software Spectroscopic Ellipsometry Analyzer (SEA) (Csermely et al., 2012) from Semilab® to obtain the optical parameters and film thickness.

Figure 1. Ellipsometric three-phase model used.

Phase 3
Anodized film (Phase 2) and air
Phase 2
Anodized film (dispersion laws)
Phase 1
Substrate + natural oxide (n-k file)

Figure1 details the used model composition. Source: Authors (2020).

A three-phase model (Figure 1) was designed to cope with films characteristics to calculate the optical parameters and film thickness. Figure 1 depicts model characteristics. The phases were a substrate upon which resides a naturally grow titanium oxide (Phase 1), described by an nk-file. A titanium oxide film grown by anodization (Phase 2), described by dispersion laws (basically Cauchy and Tauc-Lorentz), and a mix of Phase 2 and air (Phase 3), modeled using EMA (Fujiwara, 2007) to take into account surface roughness.

2.3 Surface topography and roughness

The surface topography and surface roughness of titanium anodized samples at 20 V, 40 V, 60 V and 80 V were investigated by an atomic force microscope Nanosurf Flex AFM® instrument. Samples were scanned in a contact mode and in air at room temperature. The anodized titanium images were carried out in a 20 nm x 20 nm (400 nm^2) scanned area. The average roughness (Ra) and the root mean square (Rq) parameters, as well as its standard deviations were calculated for five distinct points across the sample surface.

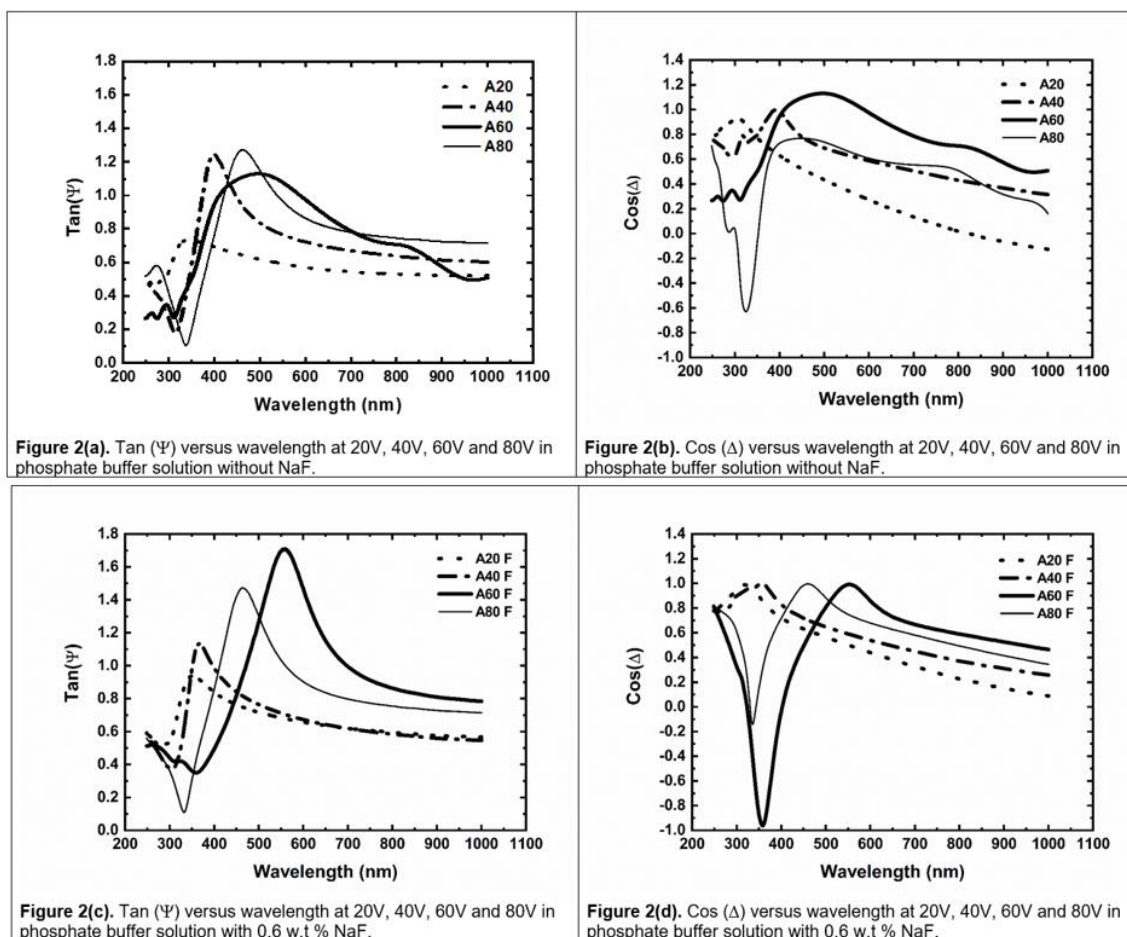## 2.4 Electrochemical impedance spectroscopy

Electrochemical impedance spectroscopy (EIS) was carried out with the aim of studying the fluoride influence in anodized samples during corrosion. Furthermore, EIS technique allowed us to estimate the anodized oxides thickness to compare with those obtained by spectroscopic ellipsometry. The variation of the open circuit potential (OCP) was registered for 30 minutes before EIS tests in the same electrolyte. EIS was performed using potentiostatic/galvanostatic Autolab® PGSTAT 204 with frequency response analysis module FRA32M and NOVA 2.1 software. The spectra were recorded at three-cell electrodes, using

Ag/AgCl/KClsat. as a reference electrode and a platinum wire as counter-electrode in frequency ranging from 100 KHz to 10mHz with AC potential of 10 mV. The experimental data were fitted, using the Z-view® software. The fitting of the equivalent electrical circuits was considered satisfactory when the sum of squared deviation (χ^2) values were equal or less than 10^{-3} and the percentual error related to each element of the circuit was less than 20% (Macdonald, 1988).

3. Results

3.1 Optical Properties and thickness

Figure 2. Ellipsometric parameters tan (Ψ) and cos (Δ) versus wavelength for different apllied anodizing potentials.

Figure 2(a). Tan (Ψ) versus wavelength at 20V, 40V, 60V and 80V in phosphate buffer solution without NaF.

Figure 2(b). Cos (Δ) versus wavelength at 20V, 40V, 60V and 80V in phosphate buffer solution without NaF.

Figure 2(c). Tan (Ψ) versus wavelength at 20V, 40V, 60V and 80V in phosphate buffer solution with 0.6 w.t % NaF.

Figure 2(d). Cos (Δ) versus wavelength at 20V, 40V, 60V and 80V in phosphate buffer solution with 0.6 w.t % NaF.

Figures 2(a) and 2(b) show the results the ellipsometric parameters tan (Ψ) and cos (Δ) in a phosphate buffer solution without NaF (A20, A40, A60, A80), and Figures 2(c) and 2(d) show the results the ellipsometric parameters tan (Ψ) and cos (Δ) in a phosphate buffer solution with 0.6 w.t % NaF (A20 F, A40 F, A60 F, A80 F). Source: Authors (2020).

Figure 2 shows the variation of the ellipsometric parameters tan (Ψ) and cos (Δ) for different anodizing potentials, in both phosphate buffer solutions. As expected, as we increase the values of potential applied, the oscillations of both parameters increase as observed by Fujiwara (2007), confirming a greater thickness. In each subfigure there is detail about of its content.

Figure 3. Refractive index (n) versus anodization potential apllied (V) at λ = 700 nm, for both phosphate buffer solutions, without NaF and 0.6 w.t %.
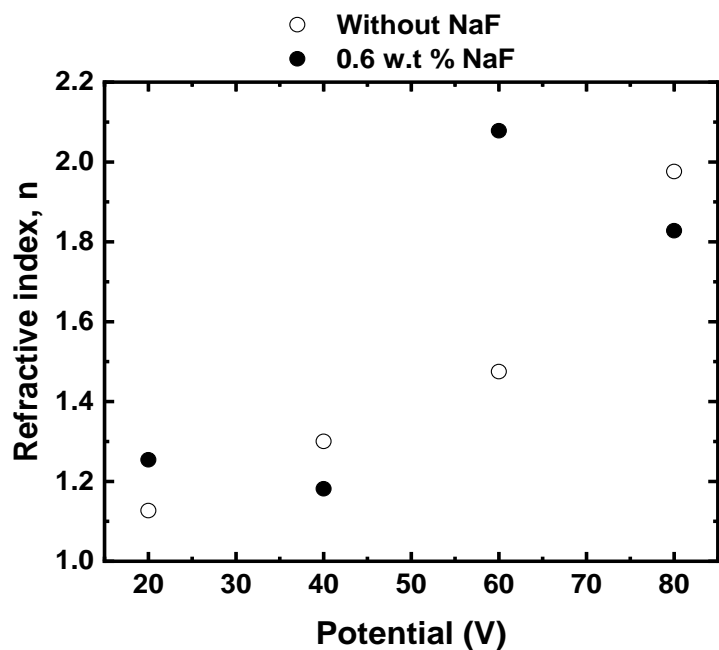
Figure 3 shows refractive index data for the solution without NaF in open circles, and refractive index data for the solution with 0.6 w.t % NaF in full circles. Source: Authors (2020).

Figure 3 exhibits the refractive index (n) values of anodic grown oxides at wavelengh of 700 nm. Despite the fluctuations, there is a general tendency of growth of n as V increases. The solution without NaF increases steadily in the voltage range observed. The growth of the refractive index of TiO_2 at 700 nm as anodization potential is applied was also observed by Sapoletova et al. (2019) in a different solution in the range of 35 V to 50 V.

Figure 4. Thickness versus anodization potential, obtained by SE, for both phosphate buffer solutions, without NaF and 0.6 w.t %.
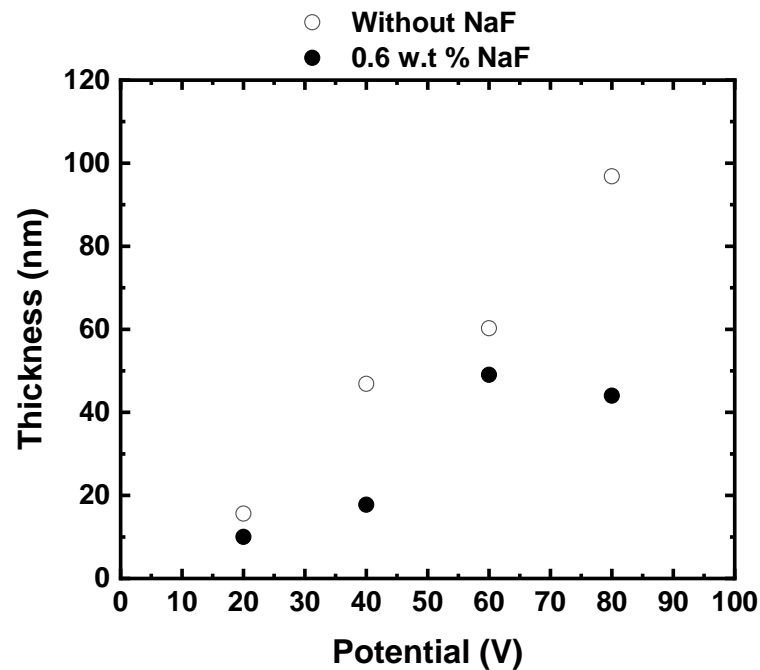
Thickness as a function of the anodizing potential applied. Measures from solutino without NaF is shown in open circles, and with 0.6 w.t % NaF is show in full circles. Source: Authors (2020).

The oxide thickness as function of the anodized potential values obtained by ellipsometry is presented in Figure 4 for both phosphate buffer solutions without NaF, and with 0.6 w.t % NaF. The thickness of titanium oxides films anodized with the solution containing fluoride are lower than the ones grown without NaF. The thickness for oxides grown without NaF appears to be a linear function of the applied potential, with R2 of 0.97 and with a growth rate of roughly (1.3 ± 0.2) nm/V, which, considering the error bar, is in accordance with the values obtained by Liu et al. (2016). With the same condition, it is also in the range of the values expected by Diamanti et al. (2011). On the other hand, in the solution with NaF at 80V, one may interpret the curve has a change in curvature, which, in this case, it could possibly be due to a film dielectric breakdown (Saldanha et al., 2020). In this solution (with 0.6 w.t % NaF) the lower anodization constant could also be associate to the presence of fluoride ions that collaborates with the dissolution of the oxide film at all potentials applied (Kong, 2008).

3.2 Surface topography and roughness

Table 2. Influence of fluoride anion incorporated during anodization on titanium anodized surface average roughness values obtained by AFM.
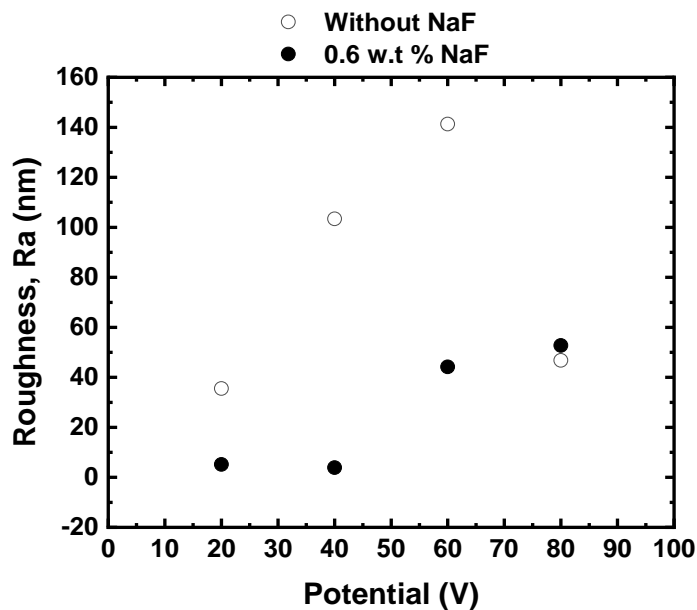
without NaF					with 0.6 w.t % NaF				
Sample	Ra	Sd (Ra)	Rq	Sd (Rq)	Sample	Ra	Sd (Ra)	Rq	Sd (Rq)
A20	36	2	47	5	A20 F	5.1	0.4	6.5	0.5
A40	103	6	116	6	A40 F	3.9	0.2	5.0	0.6
A60	141	9	180	10	A60 F	44	2	53	3
A80	47	4	61	4	A80 F	53	4	64	4

Ra stands for average roughness. Rq is the root mean square average. Sd is the standard deviation of the corresponding measure. Source: Authors (2020).

The roughness values we obtained using the AFM as a function of the anodization potentials are shown in Table 2. Ra stands for average roughness, i.e., it is the arithmetic average of the absolute values of the profile heights over the evaluation lengh, while Rq is the root mean square average of the same parameter, also over the evaluation lengh. Sd is the standard deviation of the measure.

According to Table 2, it can be observed that the films obtained with NaF have lower roughness values than those anodized without NaF. Roughness tends to increase as applied potential grows.

Figure 5. Roughness versus anodization potential apllied in both phosphate buffer solutions, without NaF and 0.6 w.t %.


Results of roughness, Ra (nm), as a function of the anodizing potential applied. Without NaF is shown in open circles, and with 0.6 w.t % is show in full circles. Source: Authors (2020).

Figure 5 showns average roughness Ra as function of the applied anodization potential. Disregarding, the flutuactions and the drop at 80 V, for the film grown with NaF, the remaining values suggest a growth in surface roughness as anodizing potential increases. The rougher surfaces usually improve biological funcions as osteogenic differentiation, as observed by Kim et al. (2006).

According to Vera et al. (2017), the characteristics required for oxide film in contact with blood is a level of roughness (Ra) lower than 50 nm, because it can avoid the promotion of blood clots. In our study, the coating roughness (Ra) were lower than 50 nm in the presence of the NaF in solution.

Figure 6. AFM images of anodized titanium surfaces at different applied potentials for both solutions, without NaF and 0.6 w.t %.
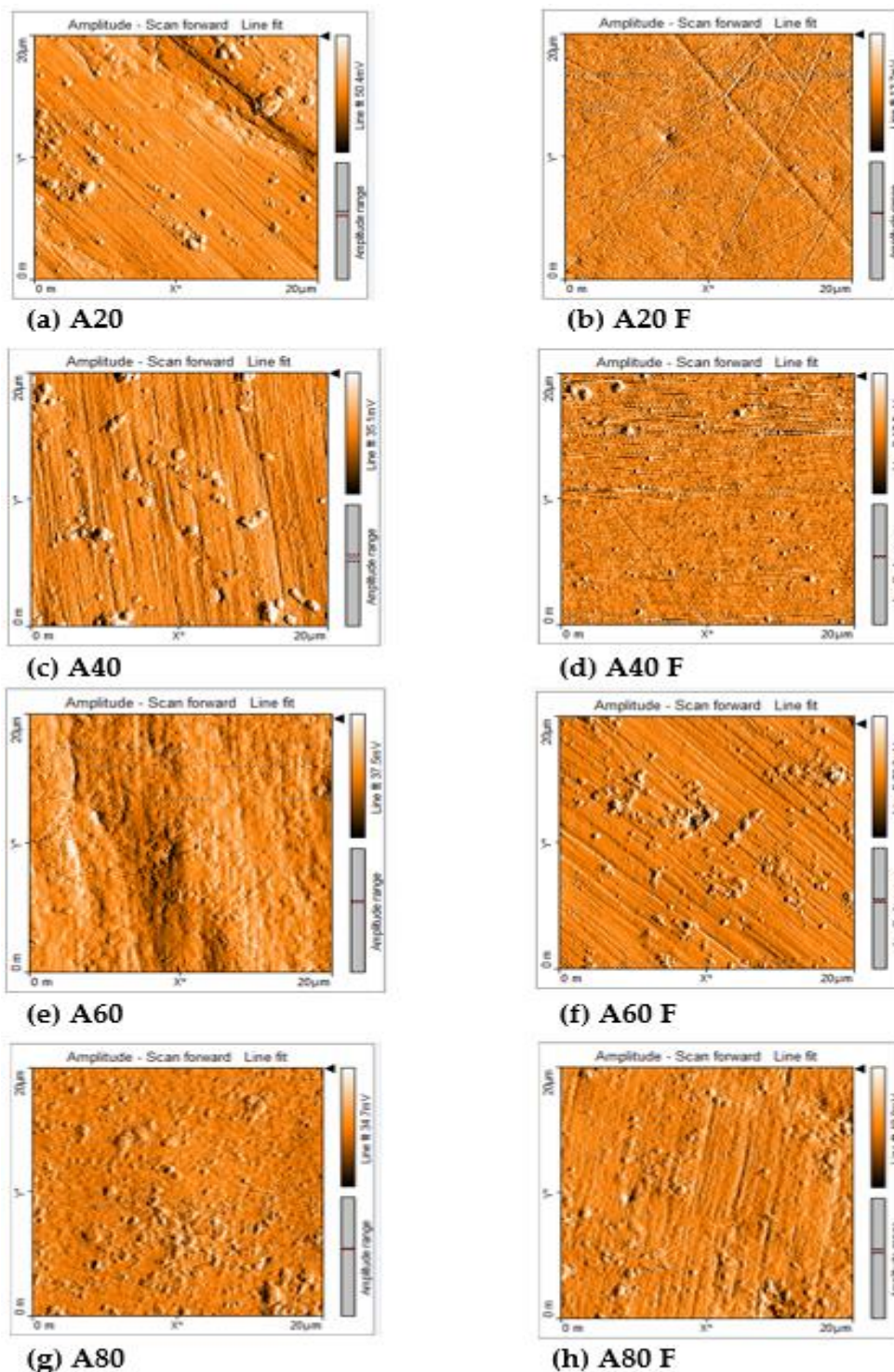
AFM images. Samples anodized in phosphate buffer solution with 0.6 w.t % NaF appear with a capital F at the end of its name, which includes a direct reference of the applied potencial. Source: Authors (2020).

Surface topography was evaluated with AFM. Figure 6 shows the surface topography of the samples surface for both solutions. It is also possible to observe scratches on anodized surface samples remaining from mechanical grinding and polishing processes. It is noticeable that almost all the surfaces which were in contact with the solution with NaF are smoother than the ones in contact with solution with NaF.

Comparing subfigures side by side, in both columns, we could argue that the appearance of surface sample A20 F is smooother than the one of A20. The same is clear when comparig A40 and A40 F. For A60 and A60 F the difference seems more tricky, but one can notice the longer surface wavelength, as a deep valley is more visible in A60. It appears darker in the image. Equally A80 and A80 F seem to be more similar. This behavior is in accordance with roughness value obtained by AFM, presented in Figure 5. Beyond that, globular structures are clearly present on most surfaces of Figure 6. They were was also reported by Gomez Sanchez et al. (2013), as they obtained contact mode AFM images of titainum anodized in phosphoric acid solution at 18 V, and 30 V. Xing et al. (2013) also observed the onset of "nodule-like" or "flower-like" structures for anodization in $0.1mol.L^{-1}$ H_2SO_4 at 30V, which they claim to be mainly composed of TiO_2 crystalline grains.

3.3 EIS measurements

Since the films formed in phosphate buffer solutions with 0.6 w.t % NaF presents lower thickness as function of the applied anodizing potential, and their surface roughness are less than 50 nm, they fulfill the requirements necessary to avoid the promotion of blood clots, according to Vera et al. (2017) which ultimately can promote thrombosis. Once studies such as (Kong, 2008; Wang et al., 2016; Fukushima et al., 2018) have indicated that the Titanium oxide that incorporates fluoride anions still presents biocompatibility, it would be wise to analyze the corrosion resistance the oxide films formed in a phosphate buffer solution with 0.6 w.t % NaF presence, using EIS measurements. The results were interpreted, using the Bode Diagrams (Macdonald, 1988) and, from the EIS measurements, the thicknesses also were determined and compared with those obtained by elllipsometry.

Figure 7. Bode diagrams: (a) -θ versus log f and (b) log |Z| versus log f for Ti anodization in phosphate buffer solution with 0.6 w.t % at different anodization potentials applied.
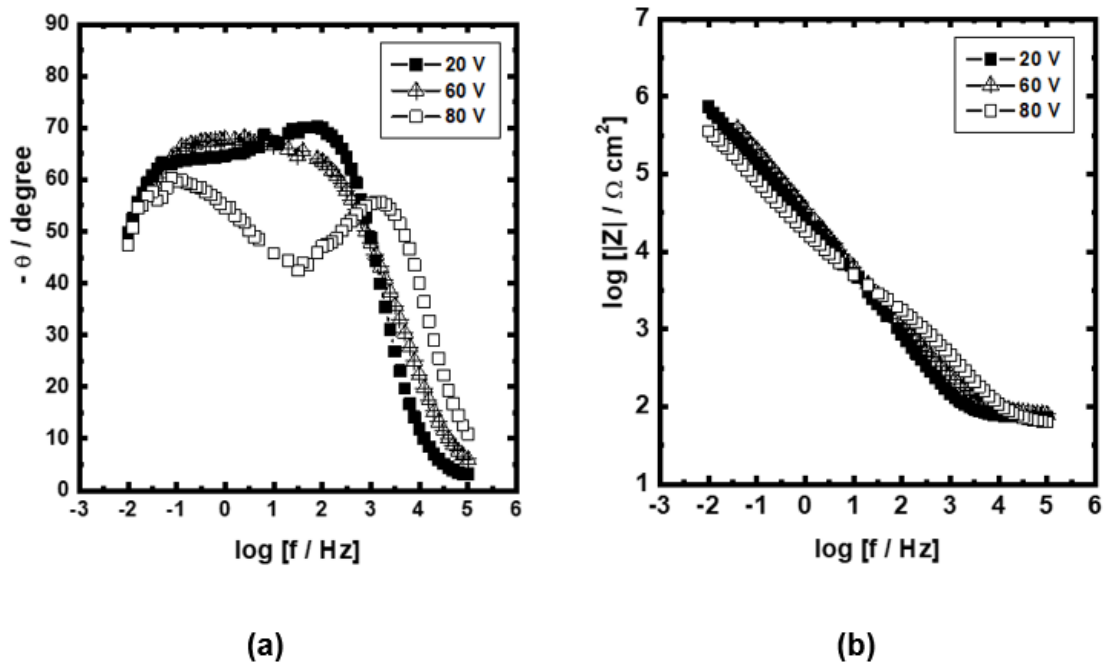
Bode diagrams for A20 F, A60 F and A80 F. Source: Authors (2020).

Figure 8. Equivalent electrical circuits (EEC) used to fit the impedance data of the oxide films formed at different potentials applied (a) 20 V (sample A20 F) and 80 V (sample A80 F), and at (b) 60 V (sample A60 F) in phosphate buffer solution with 0.6 w.t %.
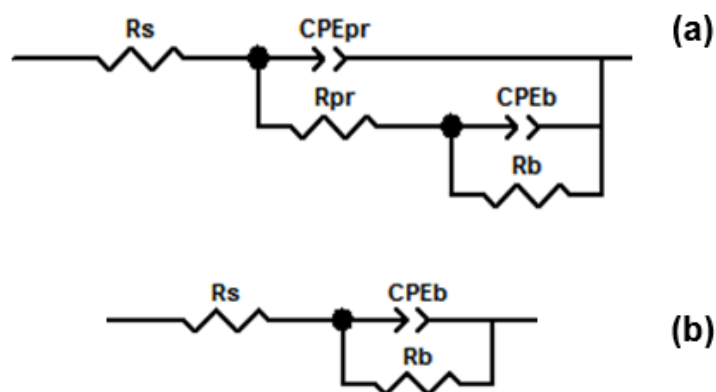
R_s, R_{pr}, CPE_{pr}, CPE_b, and R_b are the resistance of the solution, the resistance of the porous layer, the constant phase element of the porous layer, the constant phase element of the barrier layer, and the resistance of the barrier layer, respectively. Source: Authors (2020).

Figures 7 present the Bode diagrams represented by - θ versus log f (A) and log |Z| versus log f (B), where θ, |Z|, and f are the phase angle, the impedance module, and the frequency, respectively. The Bode diagrams for oxide films formed at 20 V and 80 V present two time constants. The first time constant is located at high frequencies, between 10^3 Hz and 10 Hz for the film formed at 20 V, and between 10^5 Hz and 10^2 Hz for the film formed at 80 V. This time constant can be associated with the response of the outer porous layer denominated by pr. On the other hand, the second time constant was detected at frequencies lower than 10 Hz for the oxide film formed at 20 V, and at 10^2 Hz for the oxide films formed at 80 V. This one can be associated with an inner barrier layer denominated b. Consequently, these results suggest that these oxide films on the titanium present double-layer structures (J.-H. Xing et al., 2013).

These impedance results for the oxide films formed at 20 and 80 V were fitted by the equivalent electrical circuit (EEC) shown in Figure 8(a), which used constant phase elements (CPE). The CPE represents the non-ideal capacitive response related to the heterogeneity of the studied systems (Orazem & Tribollet, 2008). In the circuit depicted in Figure 8(a), Rs is associated with the solution resistance, CPEpr and Rpr to the constant phase element and resistance of the porous layer, and CPEb and Rb to the constant phase element and resistance of the barrier layer.

For the oxide film formed at 60 V, the impedance responses showed in Figures 7(a) and 7(b) can be fitted by the circuit shown in Figure 8(b). This circuit indicates that the oxide film on the titanium presents a single-layer structure, where Rs, CPEb, and Rb have the same definition as for Figure 8(a).

Table 3. Equivalent electrical circuit parameter values obtained from fitting of the EIS experimental data of the oxide films formed at different potentials applied.

Potential (V)	R_s (Ω cm^2)	CPE_{pr} (μF cm^{-2} s$^{\alpha-1}$)	n	R_{pr} (kΩ cm^2)	R_b (kΩ cm^2)	CPE_b (μF cm^{-2} s$^{\alpha-1}$)	n	χ^2 (10^{-3})
20	72.18 (0.39)	5.03 (1.87)	0.85 (0.29)	19.94 (7.75)	2581.5 (5.24)	5.04 (1.73)	0.67 (0.88)	0.69
60	78.68 (0.83)	-	-	-	4006.7 (17.23)	7.05 (0.69)	0.75 (0.17)	2.15
80	56.18 (1.07)	2.68 (4.35)	0.77 (0.59)	3.06 (3.44)	1978.9 (9.22)	13.81 (1.03)	0.66 (0.51)	1.0

Fitting data for (a) 20 V (sample A20 F) and 80 V (sample A80 F), and at (b) 60 V (sample A60 F) in phosphate buffer solution with 0.6 w.t % NaF. The error % related to each element of the circuit is given inside parentheses. Source: Authors (2020).

Table 3 resumes all the parameter values in the equivalent electrical circuit. Particularly, in table 3, the values of the adjust parameter n (not to confuse with refraction index) can be 1, 0.5 or in the range $0.5 \leq n \leq 1$. The value 1 corresponds to the response of an ideal capacitor C. The value 0.5 can represent a diffusion response at low frequencies, and the values between $0.5 < n < 1$ are associated with a heterogeneous distribution of the properties of the oxide (Macdonald, 1988).

4. Discussion

The films obtained by anodizing in a phosphate buffer solution containing 0.6 w.t % NaF presented more defined ellipsometric spectra peaks. The appearance of the curves for both parameters, tan (Ψ) and cos (Δ), measured from samples treated with NaF, is more regular than those measured from samples grown without NaF. The oscillations appear to increase as applied voltage grows, indicating a larger thickness. The incorporation of fluoride ions in the film during anodizing probably inhibited the increase of both thickness and

roughness of the titanium oxide film, although enhancing biocompatibility. Particularly the lower values of surface roughness (Ra < 50 nm) are a good result, once it avoids the formation of blood clots (Vera et al., 2017).

It was also observed that refractive index (n) increases with increasing anodizing applied potential. The higher values at 60 V and 80 V are probably due to the oxide film transition from amorphous to crystalline structure or a mixture of rutile and anatase (J.-H. Xing et al., 2013). Globular structures were also observed by AFM images in all anodized samples that suggest crystalline structures formation (Saldanha et al., 2020).

Regarding the EIS study, the change of the oxide film structure from the double-layer (for the film formed at 20 V) to the single-layer (for the oxide film formed 60 V), it is not known the exact mechanism responsible for it. The oxide film can undergo numerous processes during the anodization as function the potential, such as changes of the surface topography, presence or develop of crystal structures, oxide dissolution, oxygen evolution, and anionic incorporation in the oxide films (Sul et al., 2001). Consequently, these different factors can be responsible for this structural change.

Finally, the structural evolution of the oxide film from a single layer (for the oxide film formed at 60 V) to double-layer (for the oxide film formed at 80 V) can be associated principally with a possible dielectric breakdown of the film at 80 V. The thicknesses (L) of the passive layers were calculated using the values of the CPE of the compact barrier layer (CPEb for the film with a single layer structure) or porous layer (CPEpr for the films with double-layer structure) and their respective n values (not refractive index), related to the capacitance, and Rs of the electrolyte resistance (Table 3) (Hernández-López et al., 2015):

$$L = \varepsilon \varepsilon_0 \, A / [CPE^{\frac{1}{n}} . Rs^{\frac{(1-n)}{n}}] \qquad (1)$$

where A is the effective surface area, ε is the dielectric constant of TiO_2 and has been estimated assuming the value 25.2 (Hernández-López et al., 2015), ε_0 is the vacuum permittivity, and L is the passive film thickness. The Rs parameter is used when the oxide resistance becomes infinitely large.

Table 4. Oxide film thickness as function of the applied potential obtained by EIS and SE.

Thickness (nm)		
Sample	**Technique**	
	EIS	*SE*
A20 F	17.63	10.03
A40 F	Error	17.75
A60 F	40.42	44.01
A80 F	115.69	49.04

Source: Authors (2020).

Figure 9. Thickness versus apllied potential.
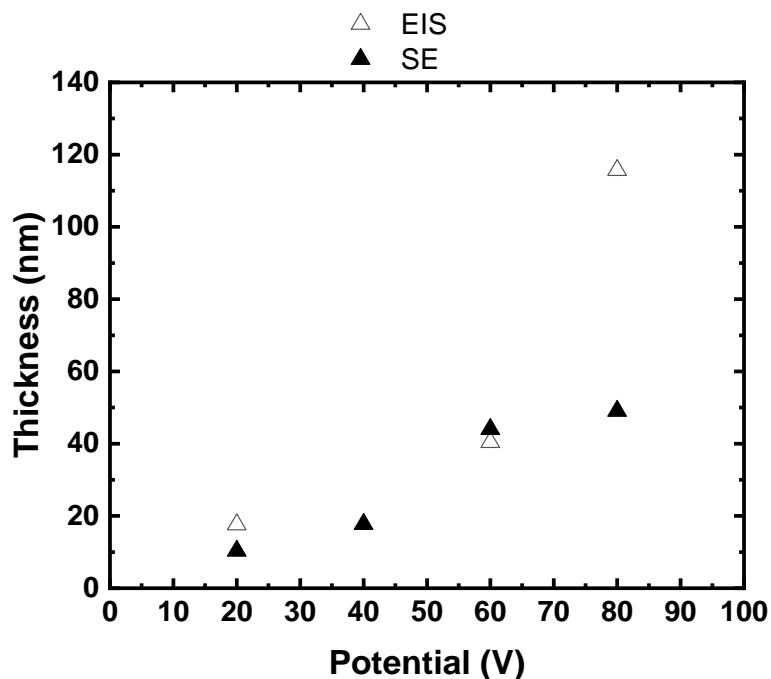
Thickness obtained by EIS are shown in open triangle, and by SE in full triangle. Source: Authors (2020).

Table 4 shows the oxides film thickness obtained by electrochemical impedance spectroscopy (Eq. 1) and spectroscopic ellipsometry (from Figure 4). Unfortunately, sample A40 F yielded a non-recovery error. In Figure 9, thickness from EIS and SE are plotted as function of the applied potential.

The thickness values accessed from the EIS and SE techniques better agree for 20 V and 60 V. The anodized oxide film thickness increases with the applied potential. The greatest thickness value was 115.69 nm, obtained by EIS at 80 V, a lower value than that obtained

when anodized in a sulfuric acid solution (Karambakhsh et al., 2011).

However, this value is far superior to the one obtained by SE. The discrepancy can be understood once, possibly dielectric breakdown may have taken place at 80 V. In this case, as dielectric constant changes, it can affect directly ellipsometric measurements once they are based on film optical properties (Fujiwara, 2007). The oxide film formed at 60 V was the most corrosion-resistant (Table 3). On the other hand, at 80 V, a dielectric breakdown possibly left the film more porous and less corrosion resistant.

5. Conclusion

In this paper we investigated the effect on topography, roughness, optical properties, and thickness of anodized titanium film at different potentials. We showed that surfaces treated with NaF, generally, are less rough than the ones treated without NaF. The surface roughness values are less than 50 nm, which is good for avoiding the formation of blood clots. Film thickness of surfaces which fluoride anions incorporated on it are usually thinner than those obtained in phosphate buffer solution without NaF. Topography analysis showed the presence of what appears to be globular-like structures in oxides anodized in both solutions. Considering the film anodized in the phosphate buffer solution with 0.6 w.t % NaF, the EIS and SE techniques converge in the obtained thickness values at 20 V and 60 V, once they are closer to each other. At 60 V, the film presented the best corrosion resistance behaviour, and the worst performance was observed at 80 V, which can be due to a possible film dielectric breakdown. Finally, we stress that the oxide films formed in solution with NaF presence presented smaller thickness, lower surface roughness (Ra ≤ 50 nm), and excellent corrosion resistance.

The authors intend to study the effect of the fluoride concentration on the same parameters (thickness, roughness, corrosion resistance) analysed in this article. Also, we plan to investigate the actual composition of thin film, using techniques such as XPS and LIBS, to better evaluate the fluoride anions incorporation to the film, as a function of the applied potential.

Acknowledgements

References

Aladjem, A. (1973). Anodic oxidation of titanium and its alloys. *Journal of Materials Science*, *8*(5), 688–704. https://doi.org/10.1007/BF00561225

Blackwood, D. J., Greef, R., & Peter, L. M. (1989). An ellipsometric study of the growth and open-circuit dissolution of the anodic oxide film on titanium. *Electrochimica Acta*, *34*(6), 875–880. https://doi.org/10.1016/0013-4686(89)87123-3

Csermely, Z., Horvath, Z., Hanyecz, I., & Lugosi, L. (2012). *Spectroscopic Ellipsometry Analyser: User 's Reference Manual*. 158.

Diamanti, M. V., del Curto, B., & Pedeferri, M. (2011). Anodic oxidation of titanium: From technical aspects to biomedical applications. *Journal of Applied Biomaterials and Biomechanics*, *9*(1), 55–69. https://doi.org/10.5301/JABB.2011.7429

Diamanti, M. V., & Pedeferri, M. P. (2007). Effect of anodic oxidation parameters on the titanium oxides formation. *Corrosion Science*, *49*(2), 939–948. https://doi.org/10.1016/j.corsci.2006.04.002

Fovet, Y., Gal, J., & Toumelin-chemla, F. (2001). Influence of pH and fluoride concentration on titanium oxide. *Talanta*, *53*, 1053–1063.

Fujiwara, H. (2007). *Spectroscopy Ellipsometry. Principles and Applications*. Tokyo: Maruzen Co. Ltd.

Fukushima, A., Mayanagi, G., Sasaki, K., & Takahashi, N. (2018). Corrosive effects of fluoride on titanium under artificial biofilm. *Journal of Prosthodontic Research*, *62*(1), 104–109. https://doi.org/10.1016/j.jpor.2017.08.004

Gomez Sanchez, A., Schreiner, W., Duffó, G., & Ceré, S. (2013). Surface modification of titanium by anodic oxidation in phosphoric acid at low potentials. Part 1. Structure, electronic properties and thickness of the anodic films. *Surface and Interface Analysis*, *45*(6), 1037–1046. https://doi.org/10.1002/sia.5210

Hernández-López, J. M., Conde, A., de Damborenea, J., & Arenas, M. A. (2015). Correlation of the nanostructure of the anodic layers fabricated on Ti13Nb13Zr with the electrochemical impedance response. *Corrosion Science*, *94*, 61–69. https://doi.org/10.1016/j.corsci.2015.01.041

Huang, X., & Liu, Z. (2013). Growth of titanium oxide or titanate nanostructured thin films on Ti substrates by anodic oxidation in alkali solutions. *Surface and Coatings Technology*, *232*, 224–233. https://doi.org/10.1016/j.surfcoat.2013.05.015

Karambakhsh, A., Afshar, A., Ghahramani, S., & Malekinejad, P. (2011). Pure commercial titanium color anodizing and corrosion resistance. *Journal of Materials Engineering and Performance*, *20*(9), 1690–1696. https://doi.org/10.1007/s11665-011-9860-0

Kim, M. J., Choi, M. U., & Kim, C. W. (2006). Activation of phospholipase D1 by surface roughness of titanium in MG63 osteoblast-like cell. *Biomaterials*, *27*(32), 5502–5511. https://doi.org/10.1016/j.biomaterials.2006.06.023

Kong, D. S. (2008). The influence of fluoride on the physicochemical properties of anodic oxide films formed on titanium surfaces. *Langmuir*, *24*(10), 5324–5331. https://doi.org/10.1021/la703258e

Liao, M., Ma, H., Yu, D., Han, H., Xu, X., & Zhu, X. (2017). Formation mechanism of anodic titanium oxide in mixed electrolytes. *Materials Research Bulletin*, *95*. https://doi.org/10.1016/j.materresbull.2017.08.041

Liu, Z. J., Zhong, X., Walton, J., & Thompson, G. E. (2016). Anodic Film Growth of Titanium Oxide Using the 3-Electrode Electrochemical Technique: Effects of Oxygen Evolution and Morphological Characterizations. *Journal of The Electrochemical Society*, *163*(3), E75–E82. https://doi.org/10.1149/2.0181603jes

Macdonald, J. R. (1988). *Impedance Spectroscopy. Theory, Experiment, and applications. phasizing solid materials and systems*. Hoboken: John Wiley & Sons, Inc.

Mardare, D., & Hones, P. (1999). Optical dispersion analysis of TiO2 thin films based on variable-angle spectroscopic ellipsometry measurements. *Materials Science and Engineering B: Solid-State Materials for Advanced Technology*, *68*(1), 42–47. https://doi.org/10.1016/S0921-5107(99)00335-9

Marino, C. E. B., Nascente, P. A. P., Biaggio, S. R., Rocha-Filho, R. C., & Bocchi, N. (2004). XPS characterization of anodic titanium oxide films grown in phosphate buffer solutions. *Thin Solid Films*, *468*(1–2), 109–112. https://doi.org/10.1016/j.tsf.2004.05.006

Orazem, M. E. & Tribollet, B. (2008). *Electrochemical Impedance Spectroscopy*. Hoboken: John Wiley & Sons, Inc.

Mazzarolo, A., Curioni, M., Vicenzo, A., Skeldon, P., & Thompson, G. E. (2012). Anodic growth of titanium oxide: Electrochemical behaviour and morphological evolution. *Electrochimica Acta*, *75*, 288–295. https://doi.org/10.1016/j.electacta.2012.04.114

Ohtsu, N., Ishikawa, D., Komiya, S., & Sakamoto, K. (2014). Effect of phosphorous incorporation on crystallinity, morphology, and photocatalytic activity of anodic oxide layer on titanium. *Thin Solid Films*, *556*, 247–252. https://doi.org/10.1016/j.tsf.2014.01.083

Pedeferri, M. (2015). Titanium Anodic Oxidation: A Powerful Technique for Tailoring Surfaces Properties for Biomedical Applications. *TMS 2015 144th Annual Meeting & Exhibition*, 515–520. https://doi.org/10.1007/978-3-319-48127-2_65

Pereira, A. S., Shitsuka, D. M., Parreira, F. J., & Shitsuka, R. (2018). Método Qualitativo, Quantitativo ou Quali-Quanti. In Metodologia da Pesquisa Científica.

https://repositorio.ufsm.br/bitstream/handle/1/15824/Lic_Computacao_Metodologia-Pesquisa-Cientifica.pdf?sequence=1.

Robin, A., & Meirelis, J. P. (2007). Influence of fluoride concentration and pH on corrosion behavior of titanium in artificial saliva. *Journal of Applied Electrochemistry*, *37*(4), 511–517. https://doi.org/10.1007/s10800-006-9283-z

Saldanha, R. L., Gomes, B. C., da Rocha Torres, G., de Lima, B. R., de Castro, J. A., da Silva, L., & Ferreira, E. A. (2020). Inhibition of the oxygen evolution reaction during titanium passivation in aqueous phosphoric acid solution. *Journal of Solid State Electrochemistry*, 16–18. https://doi.org/10.1007/s10008-020-04497-2

Sapoletova, N. A., Kushnir, S. E., & Napolskii, K. S. (2019). Effect of anodizing voltage and pore widening time on the effective refractive index of anodic titanium oxide. *Nanosystems: Physics, Chemistry, Mathematics*, *10*(2), 154–157. https://doi.org/10.17586/2220-8054-2019-10-2-154-157

Simka, W., Sadkowski, A., Warczak, M., Iwaniak, A., Dercz, G., Michalska, J., & MacIej, A. (2011). Characterization of passive films formed on titanium during anodic oxidation. *Electrochimica Acta*, *56*(24), 8962–8968. https://doi.org/10.1016/j.electacta.2011.07.129

Sul, Y.-T., Johansson, C. B., Jeong, Y., & Albrektsson, T. (2001). The electrochemical oxide growth behaviour on titanium in acid and alkaline electrolytes. In *Medical Engineering & Physics* (Vol. 23). www.elsevier.com/locate/medengphy

Tsuchiya, H., Macak, J., Sieber, I., Taveira, L., & Schmuki, P. (2006). Self-Organized Nanoporous Valve Metal Oxide Layers. In *Passivation of Metals and Semiconductors, and Properties of Thin Oxide Layers*. Elsevier B.V. https://doi.org/10.1016/B978-044452224-5/50031-7

Vera, M., Colaccio, Á., Rosenberger, M., Schvezov, C., & Ares, A. (2017). Influence of the Electrolyte Concentration on the Smooth TiO2 Anodic Coatings on Ti-6Al-4V. *Coatings*, *7*(3), 39. https://doi.org/10.3390/coatings7030039

Wang, Z. B., Hu, H. X., Zheng, Y. G., Ke, W., & Qiao, Y. X. (2016). Comparison of the corrosion behavior of pure titanium and its alloys in fluoride-containing sulfuric acid. *Corrosion Science*, *103*, 50–65. https://doi.org/10.1016/j.corsci.2015.11.003

Xing, J.-H., Xia, Z.-B., Hu, J.-F., Zhang, Y.-H., & Zhong, L. (2013). Growth and Crystallization of Titanium Oxide Films at Different Anodization Modes. *Journal of The Electrochemical Society*, *160*(6), C239–C246. https://doi.org/10.1149/2.070306jes

Xing, J., Xia, Z., Hu, J., Zhang, Y., & Zhong, L. (2013). Time dependence of growth and crystallization of anodic titanium oxide films in potentiostatic mode. *Corrosion Science*, *75*, 212–219. https://doi.org/10.1016/j.corsci.2013.06.004

Zhai, D., Du, D., & Dou, H. (2019). Effect of NaF additive on the micro/nano-structure and properties of the microarc oxidation coating on Ti6Al4V alloy. *Modern Physics Letters B*, *33*(22), 1–14. https://doi.org/10.1142/S0217984919502658

Percentage of contribution of each author in the manuscript

Gláucia Domingues – 50%

Michele de Almeida Oliveira – 10%

Nayne Barros Gonzaga Ferreira – 10%

Bhetina Cunha Gomes – 10%

Elivelton Alves Ferreira – 10%

Ladário da Silva – 10%